中国激光

铯原子激发态超窄带宽光学滤波器研究

赵韩帅[1]，杨保东[1,2,3*]，薛朝[1]，郑蓝蓝[1]

[1]山西大学物理电子工程学院，山西 太原 030006；

[2]山西大学光电研究所，量子光学与光量子器件国家重点实验室，山西 太原 030006；

[3]山西大学极端光学协同创新中心，山西 太原 030006

摘要 基于铯原子 $6S_{1/2}$-$6P_{3/2}$-$6D_{5/2}$(852 nm+917 nm)阶梯型能级结构，以波长为 852 nm 圆偏振光作为泵浦光，将原子由基态 $6S_{1/2}$ 布居到中间激发态 $6P_{3/2}$，并将原子介质极化。波长为 917 nm 线偏振光作为信号光通过极化的原子介质后，其偏振面发生了旋转，从而实现了工作波长为 917 nm 非线性光学滤波器。实验上详细测量、分析了泵浦光功率、原子气室温度，以及泵浦光与信号光同、反向实验构型对该非线性光学滤波器性能的影响，在优化的实验参数下，该滤波器的峰值透射率可达 20%，等效噪声带宽<60 MHz。超窄带宽的光学滤波器在原子钟、自由空间光通信、激光遥感系统等领域具有潜在的应用价值。

关键词 滤光器；非线性光学效应；激发态；遥感

中图分类号 O562 **文献标志码** A **DOI**：10.3788/CJL231228

1 引 言

光学滤波器常是光纤通信、量子通信、微波光子等系统中的重要组件[1-2]，基于原子介质的光学滤波器由于其带宽窄、透射率高、响应快的优点，在原子钟、自由空间光通信、激光遥感等方面具有广泛的应用价值[3-6]。基于法拉第反常色散效应的光学滤波器(FADOF)尤为常见，在理论和实验方面的研究较深入，它是基于线偏振的信号光通过磁场作用下的原子介质时其偏振方向发生旋转而实现的[7-10]。大部分 FADOF 的研究工作基于原子基态到激发态的跃迁线，这是因为原子通常处于基态，导致该 FADOF 的透射率一般较高，甚至达 90% 以上，但 FADOF 工作波长的选择性受限[11-13]。为此，基于原子激发态之间丰富的跃迁线，学者们进一步研究了激发态的 FADOF (ES-FADOF)，它常需要一束泵浦光将原子由基态激发布居到中间激发态，由于布居效率有限，其光学透射率相对 FADOF 较低，带宽通常在 GHz 量级[14-15]。窄带宽、高透射率是光学滤波器永恒的追求目标。在利用基态到激发态跃迁线实现的超窄带宽光学滤波器研究方面：基于铯原子 ^{133}Cs $6S_{1/2}(F=4)\rightarrow 7P_{3/2}(F'=5)$ 的超精细跃迁线，在弱轴向磁场(<6 G)条件下，实现了工作波长为 455 nm、峰值透射率为 9.7%、带宽为 6.2 MHz 的非线性光学滤波器[16]；基于铷原子 ^{87}Rb $5S_{1/2}(F=2)\rightarrow 6P_{3/2}(F'=3)$ 的超精细跃迁线，综合利用法拉第磁致旋光、圆二向色性、非线性饱和效应，实现了工作波长为 420 nm、峰值透射率为 2.1%、带宽为 17.8 MHz 的非线性光学滤波器[17]；为了减小多普勒效应的影响，基于铷原子 ^{87}Rb $5S_{1/2}(F=2)\rightarrow 5P_{3/2}(F'=3)$ 的超精细跃迁线，在冷原子系统中实现了工作波长为 780 nm、峰值透射率为 2.6%、带宽为 7.1 MHz 的 FADOF[18]；基于铷原子 ^{87}Rb $5S_{1/2}(F=1、F=2)\rightarrow 5P_{3/2}(F'=2)$ 三能级 Λ 型电磁感应透明系统，利用量子相干效应诱导信号光偏振面旋转，实现了工作波长为 795 nm、峰值透射率高达 33.2%、带宽为 10 MHz 的光学滤波器[19]。基于激发态之间跃迁线的非线性光学滤波器研究相对较少[20-21]，典型的工作是基于 ^{87}Rb $5S_{1/2}$-$5P_{3/2}$-$4D_{3/2}$ 阶梯型能级系统，实现了工作波长为 1529 nm、峰值透射率为 63.8%、等效噪声带宽为 546 MHz 的感生二向色性原子滤光器(IDEALF)[20]。这种 IDEALF 也在钾原子气室中实现[22-23]。

本文基于 ^{133}Cs $6S_{1/2}$-$6P_{3/2}$-$6D_{5/2}$(852 nm+917 nm)阶梯型能级系统，在波长为 852 nm 的泵浦光束与 917 nm 信号光束在铯原子气室中同向、反向重叠两种实验构型下，对 IDEALF 超窄带宽非线性光学滤波器进行了研究，结果表明二者有显著的区别。

收稿日期：2023-09-22；**修回日期**：2023-10-16；**录用日期**：2023-11-08；**网络首发日期**：2023-11-17

基金项目：国家自然科学基金(61975102)、山西省自然科学基金(20210302123437)、山西省高等学校科技创新项目(2019L0101)

通信作者：*ybd@sxu.edu.cn

2　实验原理及装置

与实验相关的铯原子能级如图 1 所示，两激发态 $6P_{3/2}$ 和 $6D_{5/2}$ 的自然线宽分别为 5.2 MHz 和 3.1 MHz。波长为 852 nm 的圆偏振光作为泵浦光，其频率通过饱和吸收光谱调谐到 $6S_{1/2}(F=4)\rightarrow 6P_{3/2}(F'=5)$ 共振跃迁线处，它将铯原子由基态超精细能级 $6S_{1/2}(F=4)$ 激发布居到中间激发态 $6P_{3/2}(F'=5)$ 的超精细能级，由于圆偏振光的作用，原子在 $6P_{3/2}(F'=5)$ 态的塞曼子能级上分布不均，即原子介质被极化。波长为 917 nm 的线偏振光作为信号光，可看成由左、右圆偏振光组成，其频率在激发态 $6P_{3/2}\leftrightarrow 6D_{5/2}$ 之间扫描，当它通过已极化的原子介质时，左旋 σ^-、右旋 σ^+ 圆偏振组分在原子介质中的吸收、色散不同，最终导致只有频率在跃迁线附近的信号光线偏振方向发生了旋转，频率远离跃迁线的信号光偏振方向几乎不旋转，从而实现了原子介质对信号光的选择性透过，即 IDEALF 光学滤波器。理论上三能级原子与两光场相互作用，在弱信号光的近似条件下，其 σ^- 圆偏振组分的极化率 χ_-[23] 可表示为

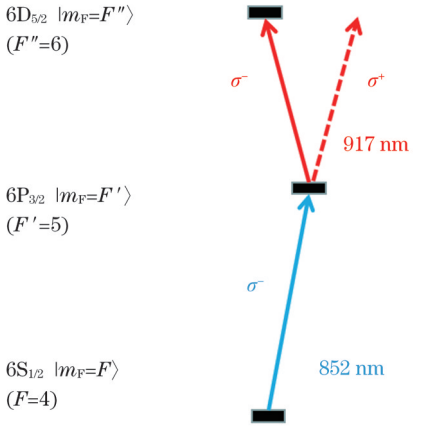

图 1　与实验相关的 ^{133}Cs $6S_{1/2}$-$6P_{3/2}$-$6D_{5/2}$ 阶梯型能级图

Fig. 1　Relevant energy levels of ^{133}Cs $6S_{1/2}$-$6P_{3/2}$-$6D_{5/2}$ ladder-type atomic system

$$\chi_-=\frac{N_0\mu_{23}^2\Omega_1^2\left[-2\gamma_{21}(\Delta_1+\Delta_2)+\gamma_2\Delta_1+\mathrm{i}(2\gamma_{21}\gamma_{31}+\gamma_2\gamma_{21})\right]}{\hbar\varepsilon_0\left\{4(\gamma_{32}+\mathrm{i}\Delta_2)\left[\gamma_{31}+\mathrm{i}(\Delta_1+\Delta_2)\right]+\Omega_1^2\right\}\left[\gamma_2(\Delta_1^2+\gamma_{21}^2)+\gamma_{21}\Omega_1^2\right]},\tag{1}$$

式中：N_0 为气室中的原子数密度；Ω_1 为泵浦光的拉比频率；μ_{23} 为 $6P_{3/2}\rightarrow 6D_{5/2}$ 的电偶极跃迁极矩；Δ_1 和 Δ_2 分别为泵浦光和信号光的频率失谐；$\gamma_{mn}=1/2(\gamma_m+\gamma_n)$ 为能态 m→n 的自发辐射衰减率；$\hbar$ 为约化普朗克常数；ε_0 为真空中介电常数。从能级图 1 可知，852 nm 圆偏振泵浦光 σ^- 将原子由基态 $6S_{1/2}$ 激发到中间激发态 $6P_{3/2}$，导致原子在中间激发态的各个塞曼子能级上分布不均衡，原子趋向于处在 $|m_F|$ 最大的子能级上。波长为 917 nm 的线偏振信号光，其左、右旋圆偏振光组分与已极化的原子介质作用的强度总是一强一弱。简化起见，忽略相互作用较弱的一项，设 σ^+ 圆偏振组分的极化率 $\chi_+\approx 0$。就一般形式，信号光的左、右旋偏振分量吸收系数之和 α 和之差 $\Delta\alpha$ 可表示为

$$\alpha=\alpha_++\alpha_-=\frac{\omega_2}{c}\mathrm{Im}(\chi_++\chi_-),\tag{2}$$

$$\Delta\alpha=\alpha_+-\alpha_-=\frac{\omega_2}{c}\mathrm{Im}(\chi_+-\chi_-),\tag{3}$$

式中：ω_2 为 $6P_{3/2}\rightarrow 6D_{5/2}$ 跃迁的角频率；c 为真空中光速。信号光偏振面旋转角 φ 可表示为

$$\varphi=\frac{\omega_2 L}{4c}\mathrm{Re}(\chi_+-\chi_-),\tag{4}$$

式中：L 为原子气室的长度。最终信号光通过滤波器的透射率 T[23] 可表示为

$$T=\frac{1}{2}\exp\left(-\frac{\alpha L}{2}\right)\left[\cosh\left(\frac{\Delta\alpha L}{2}\right)-\cos(2\varphi)\right]。\tag{5}$$

从本质上看，IDEALF 非线性光学滤波器的理论原理与原子激发态的偏振光谱是一样的，都是极化的原子介质导致线偏振光偏振面发生了旋转，区别仅是对光信号的探测方式不同而已[24-25]。

实验装置示意图如图 2 所示，泵浦光和信号光由两台光栅反馈半导体激光器提供。波长为 852 nm 的激光通过半波片（HWP）和立方偏振棱镜（PBS）光学元件分为三束。第一束用作饱和吸收光谱实验（图 2 中未画出），方便泵浦光很好地调谐到原子共振跃迁处或者将其频率锁定。第二束作为非线性光学滤波器实验中的泵浦光，其通过双色镜（DM，对 852 nm 激光反射，对 917 nm 激光透射。）与 917 nm 的信号光在铯原子气室（Cs cell 2）中同、反向重叠。气室 Cs cell 2 长度为 50 mm，直径为 25 mm，内无缓冲气体，通过聚酰亚胺电热膜和温度控制模块将其控制在室温－150 ℃左右，控温精度为 1 ℃。整个控温的 Cs Cell 2 置于一对正交的格兰-泰勒（G-T）棱镜之间，其消光比达 100000∶1，会影响到光学滤波器对背景噪声光场的抑制能力。虚线框内的部分即为光学滤波器部分，917 nm 信号光通过滤波器后在光电探测器（PD1）处，便可获得 IDEALF 非线性光学滤波器的光谱信号，定义 G-T 棱镜对偏振方向垂直时与平行时信号光强度（此时无泵浦光）的比值为光学滤波器的透射率[26]。在泵浦光与信号光同向传输的实验构型中，为了避免残余的 852 nm 泵浦光对光学滤波器信号探测的影响，在 PD1 之前，放置了一个中心

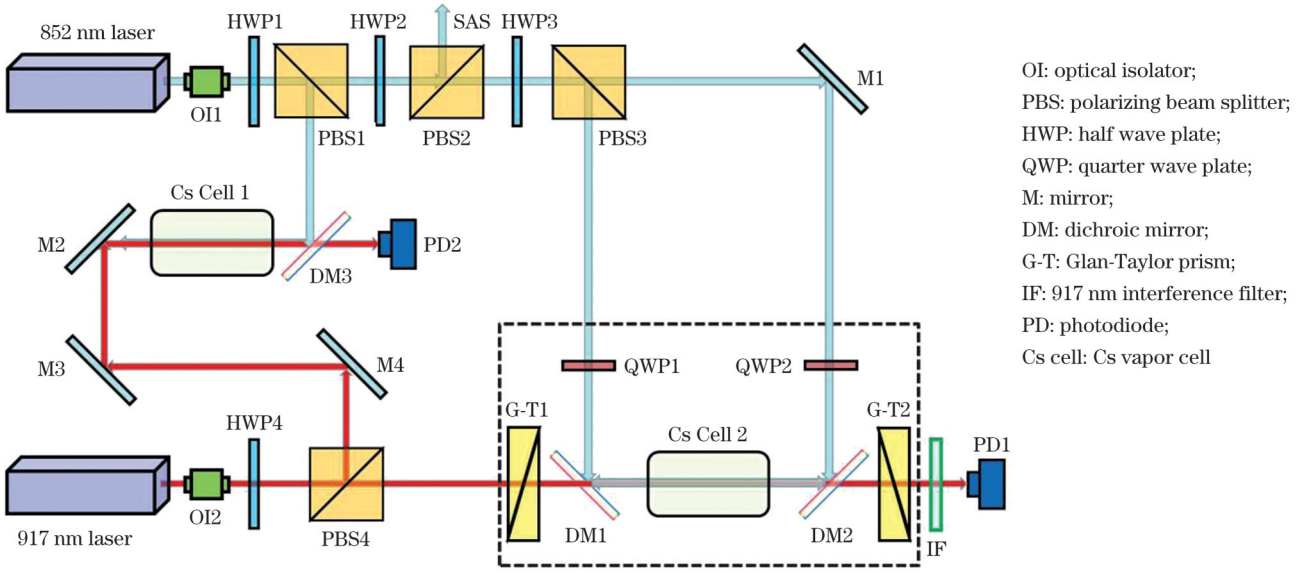

图 2　感生二向色性原子滤光器 IDEALF 实验装置示意图

Fig. 2　Schematic diagram of IDEALF experimental setup

波长为 905 nm、半峰全宽为 32 nm 的红外滤波片(IF),在 917 nm 处其透射率达 92% 以上。第三束 852 nm 激光,与一部分 917 nm 激光束在另一个原子气室 Cs cell 1 中反向重叠,在 PD2 处获得激发态 $6P_{3/2}$-$6D_{5/2}$ 超精细能级跃迁的光学双共振吸收光谱(OODR)[27-28],作为 IDEALF 非线性光学滤波器信号的频率参考。在变化实验参数时,用数字存储示波器将非线性光学滤波器信号与 OODR 光谱信号同时记录下来。

3　实验结果及讨论

当 852 nm 圆偏振泵浦光频率共振于 $6S_{1/2}(F=4)\rightarrow 6P_{3/2}(F'=5)$ 跃迁线,917 nm 信号光在激发态 $6P_{3/2}\leftrightarrow 6D_{5/2}$ 跃迁线之间频率扫描,其功率为 221 μW 时,同、反向泵浦两种实验构型下,IDEALF 非线性滤波器的典型信号如图 3 所示。在反向实验构型中,泵浦光功率为 12.2 mW,^{133}Cs 原子气室温度为 40 ℃时,获得了线翼式的 IDEALF 滤光信号,其峰值透射率达 20.9%,等效噪声带宽(ENBW)为 47 MHz;在同向实验构型中,泵浦光功率为 8.9 mW,^{133}Cs 原子气室温度为 50 ℃时,获得了单峰、共振的线芯式 IDEALF 滤光信号,其峰值透射率达 9.4%,ENBW 为 138 MHz。对于一个阶梯型的实验系统,当泵浦光与信号光在原子气室中反向重叠时,是 Doppler-free 的构型,量子相干效应导致 IDEALF 滤光信号峰值透射率较同向实验构型高一倍,且滤波器信号带宽较窄[29-31]。作为一个光学滤波器,衡量其性能的两个主要指标是透射率和等效噪声带宽,下面分别进行分析讨论。

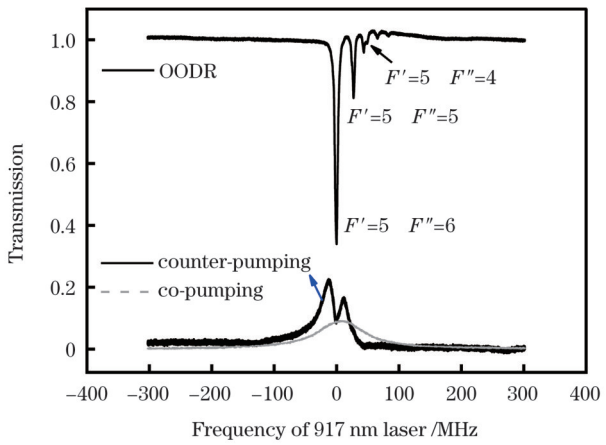

图 3　典型的 IDEALF 非线性光学滤波器光谱曲线

Fig. 3　Typical IDEALF nonlinear optical filter spectral curve

3.1　IDEALF 非线性光学滤波器的峰值透射率随实验参数的演化

图 4 为铯原子气室温度分别为 30 ℃、40 ℃、50 ℃、60 ℃时的 IDEALF 滤光信号,其他实验参数与图 3 一致。随着温度的增加,气室内铯原子数密度将会增加,圆诱导二色性效应增强,导致线偏振 917 nm 信号光旋转的角度增加,因而其峰值透射率呈上升的趋势。当温度进一步增加时,在特定的泵浦光实验参数下,处于中间激发态 $6P_{3/2}$ 上的原子数也必然增加,其对 917 nm 信号光存在吸收效应,导致峰值透射率又呈下降趋势,因此存在一个优化的原子气室温度,如图 5 所示。反向实验构型时原子气室温度为 40 ℃,同向实验构型时原子气室温度为 50 ℃,这种变化趋势与之前钾原子 IDEALF 的实验结果一致[22-23]。

激发态的原子光学滤波器性能,在很大程度上取决于中间激发态的原子布居情况。在优化的铯原子气室温度条件下,进一步测量了 852 nm 泵浦光功率对 IDEALF 非线性滤波器的影响。从图 6(a)可以看出:

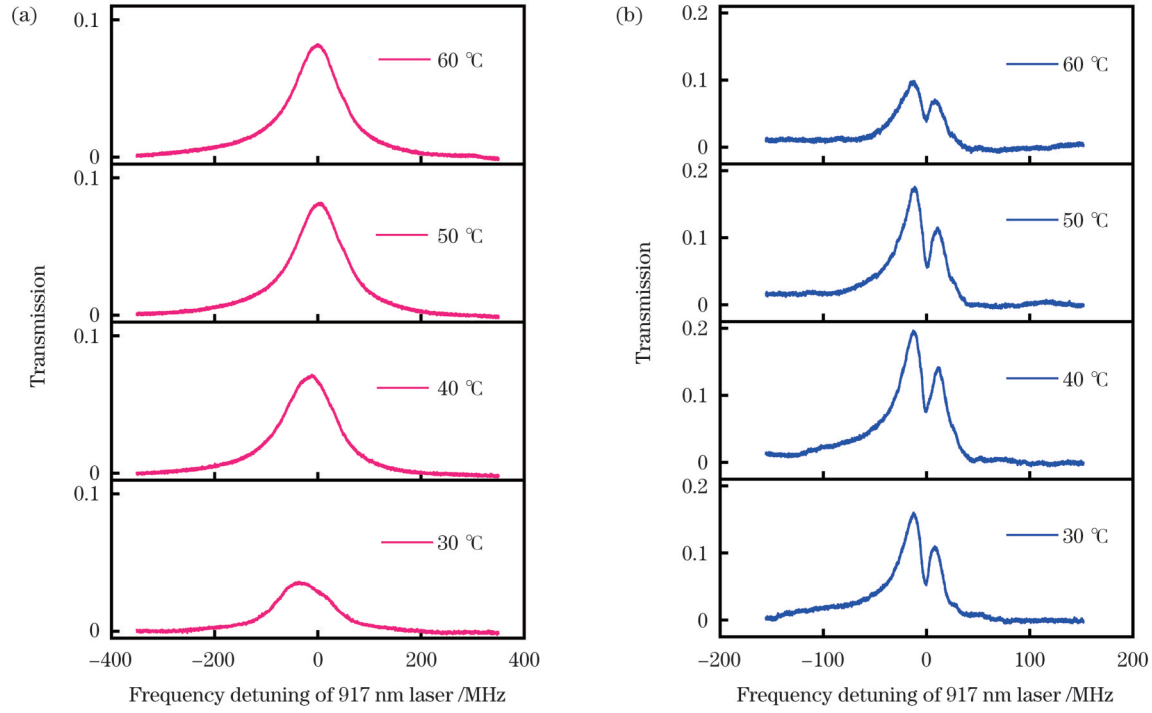

图 4 IDEALF 信号随铯原子气室温度的变化。(a)同向泵浦构型;(b)反向泵浦构型

Fig. 4 Changes of IDEALF signals with the temperature of cesium vapor cell. (a) Co-pumping configuration; (b) counter-pumping configuration

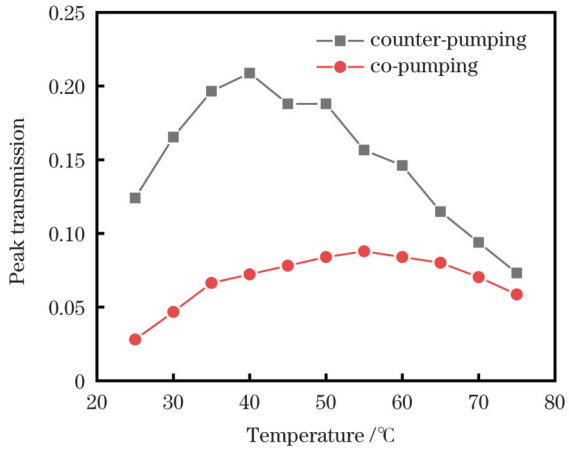

图 5 IDEALF 信号峰值透射率随铯原子气室温度的变化曲线

Fig. 5 Peak transmission of IDEALF signals with the temperature of Cs vapor cell

同向泵浦时 IDEALF 透射信号始终是一个单峰结构，即线芯式光学滤波器；反向泵浦光强较弱时，IDEALF 信号也会呈单峰结构，但随着泵浦光功率的增加，IDEALF 信号顶部分裂凹陷越来越大，呈双峰结构，逐渐过渡到线翼式光学滤波器，如图 6(b)所示，这可能是强泵浦光导致的 Aulter-Townes 分裂现象[32]。通过理论式(5)计算可知：当 852 nm 泵浦光功率比较小时 Ω_1=1.9 MHz(小于中间态 $6P_{3/2}$ 的自然线宽 5.2 MHz)，IDEALF 信号展示了单峰、共振的特征，即线芯式的滤波器；当泵浦光的功率比较大时 Ω_1=13.2 MHz，IDEALF 信号轮廓由线芯式逐步转变为线翼式滤波器，如图 7 所示。

随着泵浦光功率的增加，中间激发态 $6P_{3/2}$ 原子的布居数量增多，同、反向实验构型的滤光器峰值透射率均随之增加，如图 8 所示，且反向实验构型时 IDEALF 信号峰值透射率大于同向实验构型。

3.2 IDEALF 非线性光学滤波器的等效噪声带宽随实验参数的演化

在光学滤光器系统中，等效噪声带宽是一个非常重要的参数。理论上，可按下式计算出 IDEALF 信号的等效噪声带宽[20,33]，它表示与 IDEALF 透射信号曲线下方等面积、高度取其峰值透射率时，所对应矩形的频率范围宽度，其值越小，对背景噪声光的抑制能力越强。

$$W_{\mathrm{ENBW}}=\frac{\int_0^{\infty}S(v)\mathrm{d}v}{S(v_m)},\tag{6}$$

式中：$S(v)$为 IDEALF 信号的透射率；v 表示信号光的频率；$S(v_m)$为峰值透射率。

图 9 为在同向泵浦和反向泵浦的情况下，等效噪声带宽 ENBW 随铯原子气室温度和泵浦光功率的演化。从图 9(a)可以看出：随着温度的增加，两种实验构型的 IDEALF 信号的 ENBW 变化不明显或略有下降的趋势；随着 852 nm 泵浦光功率的增加，ENBW 呈缓慢上升的趋势，如图 9(b)所示。在现有实验参数范围下，反向泵浦的实验构型中，IDEALF 信号的 ENBW 范围为 7～60 MHz，明显窄于同向泵浦时的

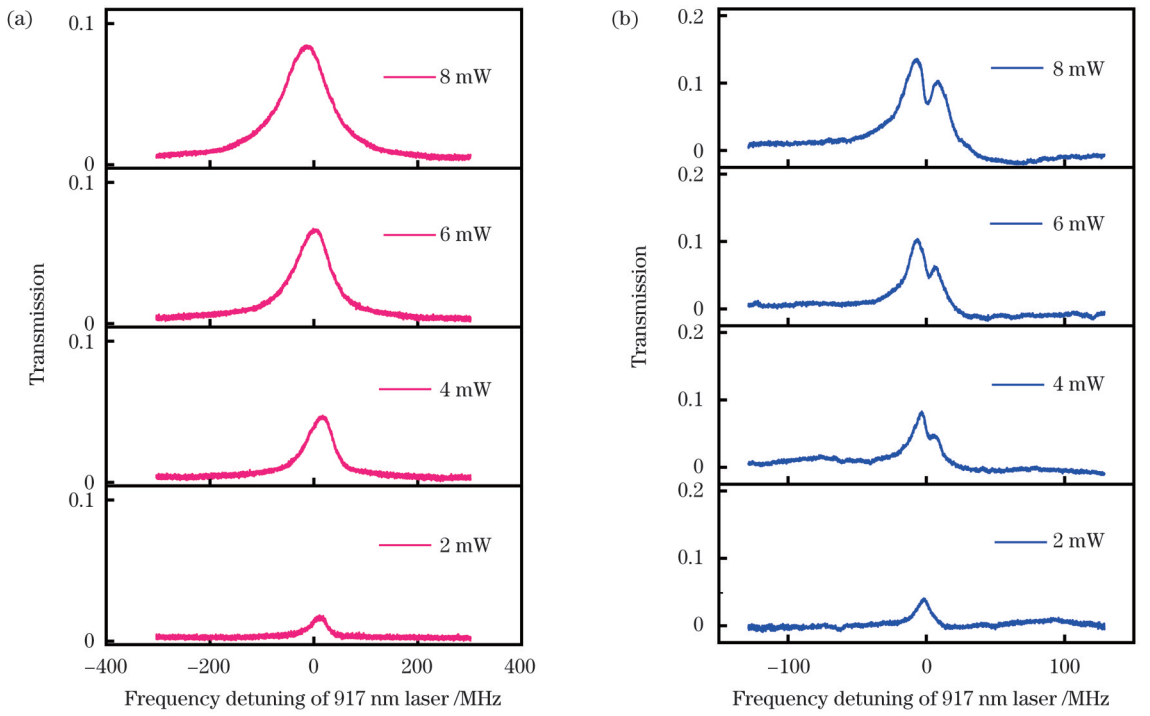

图 6 IDEALF 信号随 852 nm 泵浦光功率的变化。(a)同向泵浦构型(原子气室温度为 50 ℃);(b)反向泵浦构型(原子气室温度为 40 ℃)

Fig. 6 Changes of IDEALF signals with the power of 852 nm pump laser. (a) Co-pumping configuration (temperature of Cs vapor cell is 50 ℃); (b) counter-pumping configuration (temperature of Cs vapor cell is 40 ℃)

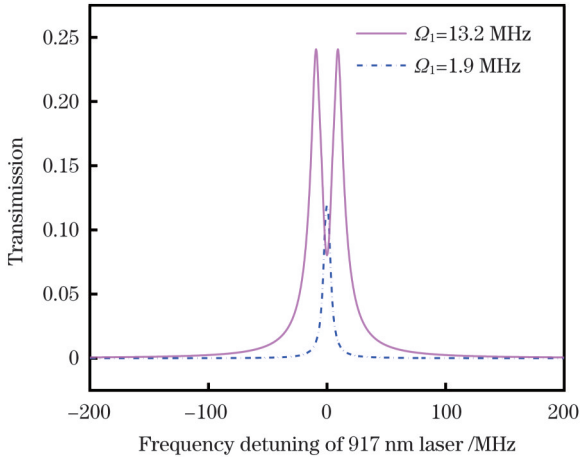

图 7 理论计算随 852 nm 泵浦光功率的增加,IDEALF 信号由线芯式向线翼式滤波器的转变

Fig. 7 Changes of IDEALF signals from line-center filter to line-wing filter with the increase of 852 nm pump optical power by theoretical calculation

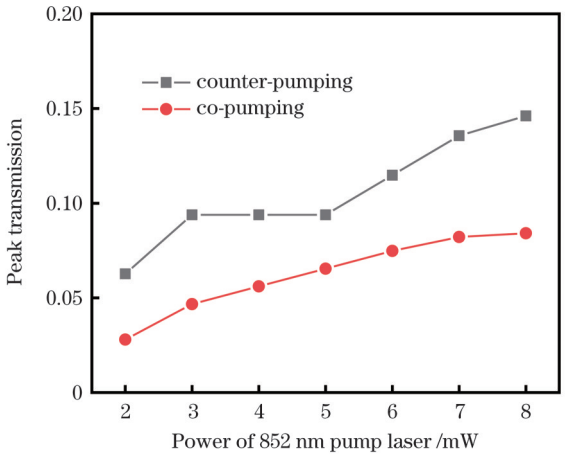

图 8 IDEALF 信号峰值透射率随 852 nm 泵浦光功率的变化曲线

Fig. 8 Peak transmission of IDEALF signals with the power of 852 nm pump laser

ENBW(90~140 MHz)。在热原子气室中,考虑 Doppler 效应,阶梯型能级系统的双光子失谐量 $\Delta=\Delta p+\Delta c+kp\cdot v+\xi\cdot kc\cdot v$,其中,$\Delta p$ 和 Δc 分别为泵浦光和信号光相对于原子跃迁线的频率失谐,kp 和 kc 为泵浦光和信号光的波矢,v 为原子在光束方向上的速度分量,$kp\cdot v$ 和 $kc\cdot v$ 为运动的原子感知到的泵浦光和信号光的 Doppler 频移量。当泵浦光与信号光在原子介质中反向传输时,$\xi=-1$,两个 Doppler 频移量在一定程度上相互抵消,此时系统是一个 Doppler-free 的构型,存在量子相干效应[29-31]。当泵浦光与信号光在原子介质中同向传输时,$\xi=+1$,与上述情形刚好相反,是一个非相干的实验系统,因此其 ENBW 较反向泵浦实验构型明显展宽。而对于三能级 Λ 型原子能级系统,泵浦光与信号光同向传输时,系统为一个 Doppler-free 的实验构型,利用电磁诱导透明(EIT)量子相干效应实现了超窄带宽、可调谐的非线性光学滤波器,如前文引言部分所述[19]。

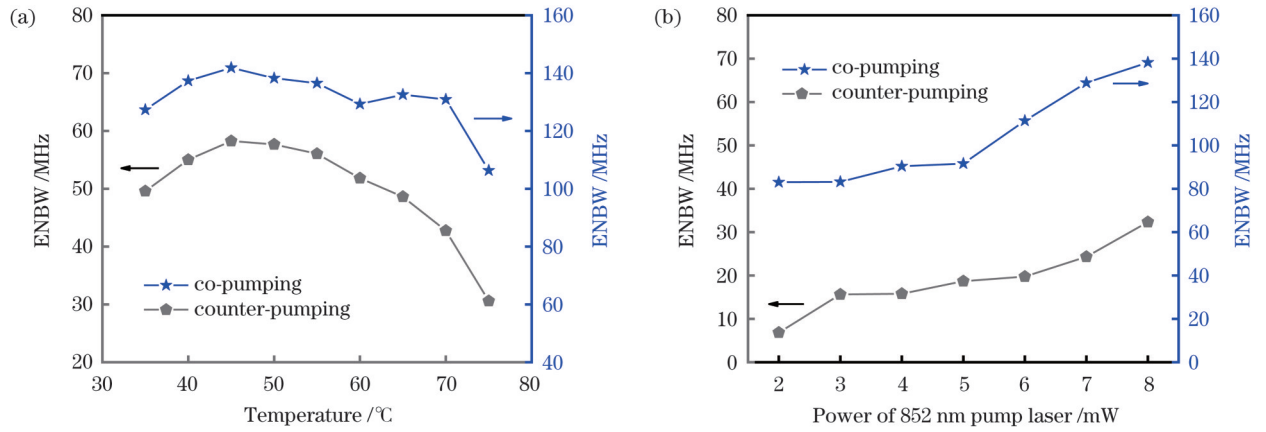

图 9 IDEALF 非线性光学滤波器信号等效噪声带宽随铯原子气室温度和泵浦光功率的变化。(a)铯原子气室温度;(b)泵浦光功率

Fig. 9 Equivalent noise bandwidth of IDEALF signal varies with the temperature of Cs vapor cell and pump light power. (a) Temperature of Cs vapor cell; (b) pump light power

4 结 论

本文基于铯原子 ^{133}Cs $6S_{1/2}$-$6P_{3/2}$-$6D_{5/2}$(852 nm+917 nm)阶梯型能级系统,测量、分析了原子气室温度、852 nm 泵浦光功率等参数对 IDEALF 非线性光学滤波器峰值透射率和等效噪声带宽 ENBW 的影响。特别是探究了泵浦光与信号光同向和反向传输时,两种实验构型的 IDEALF 滤波器的区别,实验数据表明:反向实验构型的 IDEALF 滤波器的峰值透射率更高、ENBW 更窄,多为线翼式的光学滤波器;同向实验构型的 IDEALF 信号虽透射率相对较低,ENBW 较宽,但其信号为单峰、共振于原子跃迁线的线芯式光学滤波器。从信号光传输的角度来看:线芯式的滤波器较线翼式滤波器更具有优势,因为它的透射峰是单一的,特别适合用于稳频激光、原子钟等系统;对于有多个透射峰的滤波器,如果使用一个透射峰作为信号通道,则其他透射峰为噪声通道。幸运的是,在本文反向泵浦的滤波实验中,当泵浦光的功率较小时,也可获得一个超窄线宽、单峰共振的线芯式滤波信号。总之,这两种构型下的 IDEALF 滤波器各有所长,都有相应的应用前景[34]。同时,这两种构型的 IDEALF 滤波器的 ENBW 相比传统的 FADOF 窄至少一个数量级,最窄带宽约为 7 MHz,接近铯原子中间激发态的自然线宽(5.2 MHz),且无需磁场,因此在一些无磁环境要求的场合中具有潜在的应用价值。

参 考 文 献

[1] 赖明彬, 耿敏明, 谭伊璇, 等. 基于级联微环辅助 Mach-Zehnder 干涉仪的带宽可调谐光滤波器的设计[J]. 光学学报, 2023, 43(11): 1113003.
Lai M B, Geng M M, Tan Y X, et al. Optical filter design based on cascaded double-ring-assisted Mach-Zehnder interferometers with bandwidth tuning capability[J]. Acta Optica Sinica, 2023, 43(11): 1113003.

[2] 孙良辰, 李金野, 贾倩倩, 等. 基于微环的响应可切换微波光子滤波器[J]. 激光与光电子学进展, 2023, 60(9): 0913001.
Sun L C, Li J Y, Jia Q Q, et al. Microring-based response-switchable microwave photonic filter[J]. Laser & Optoelectronics Progress, 2023, 60(9): 0913001.

[3] Tang J X, Wang Q J, Li Y M, et al. Experimental study of a model digital space optical communication system with new quantum devices[J]. Applied Optics, 1995, 34(15): 2619-2622.

[4] 猴芝玉, 杨保东, 赵韩帅, 等. 基于商用型空心阴极灯实现的法拉第反常色散原子滤光器[J]. 光学学报, 2023, 43(4): 0423001.
Gou Z Y, Yang B D, Zhao H S, et al. Faraday anomalous dispersion atomic optical filter based on commercial-type hollow cathode lamp[J]. Acta Optica Sinica, 2023, 43(4): 0423001.

[5] Popescu A, Walther T. On an ESFADOF edge-filter for a range resolved Brillouin-lidar: the high vapor density and high pump intensity regime[J]. Applied Physics B, 2010, 98(4): 667-675.

[6] 李发泉, 王玉平, 程学武, 等. 半导体激光器的原子法拉第反常色散光学滤波器光反馈稳频[J]. 中国激光, 2005, 32(10): 1317-1320.
Li F Q, Wang Y P, Cheng X W, et al. Faraday anomalous dispersion optical filter atomic frequency-stabilized semiconductor laser through optical feedback[J]. Chinese Journal of Lasers, 2005, 32(10): 1317-1320.

[7] Zhang Y D, Jia X L, Bi Y, et al. Filter performance of a cesium faraday optical filter at 852 nm[J]. Chinese Physics Letters, 2002, 19(6): 807-809.

[8] Luo B, Yin L F, Xiong J Y, et al. Signal intensity influences on the atomic Faraday filter[J]. Optics Letters, 2018, 43(11): 2458-2461.

[9] Liu Y, Yang B D, Wang J M, et al. Demonstration of Faraday anomalous dispersion optical filter with reflection configuration[J]. Chinese Physics B, 2022, 31(1): 017804.

[10] 刘双强, 掌蕴东, 何竹松. Cs 852 nm 法拉第反常色散光学滤波器研究[J]. 中国激光, 2009, 36(s1): 110-113.
Liu S Q, Zhang Y D, He Z S. Study on Cs 852 nm Faraday anomalous dispersion optical filter[J]. Chinese Journal of Lasers, 2009, 36(s1): 110-113.

[11] Ling L, Bi G. Isotope ^{87}Rb Faraday anomalous dispersion optical filter at 420 nm[J]. Optics Letters, 2014, 39(11): 3324-3327.

[12] Tao Z M, Hong Y L, Luo B, et al. Diode laser operating on an atomic transition limited by an isotope ^{87}Rb Faraday filter at 780 nm [J]. Optics Letters, 2015, 40(18): 4348-4351.

[13] Yan Y, Yuan J P, Wang L R, et al. A dual-wavelength bandpass Faraday anomalous dispersion optical filter operating on the D1 and D2 lines of rubidium[J]. Optics Communications, 2022, 509: 127855.

[14] Rudolf A, Walther T. High-transmission excited-state Faraday anomalous dispersion optical filter edge filter based on a Halbach

cylinder magnetic-field configuration[J]. Optics Letters, 2012, 37(21): 4477-4479.
[15] Sun Q Q, Hong Y L, Zhuang W, et al. Demonstration of an excited-state Faraday anomalous dispersion optical filter at 1529 nm by use of an electrodeless discharge rubidium vapor lamp[J]. Applied Physics Letters, 2012, 101(21): 211102.
[16] Wang Y F, Zhang S N, Wang D Y, et al. Nonlinear optical filter with ultranarrow bandwidth approaching the natural linewidth[J]. Optics Letters, 2012, 37(19): 4059-4061.
[17] Bi G, Kang J, Fu J, et al. Ultra-narrow linewidth optical filter based on Faraday effect at isotope ^{87}Rb 420 nm transitions[J]. Physics Letters A, 2016, 380(47): 4022-4026.
[18] Zhuang W, Zhao Y, Wang S K, et al. Ultranarrow bandwidth Faraday atomic filter approaching natural linewidth based on cold atoms[J]. Chinese Optics Letters, 2021, 19(3): 030201.
[19] Tan Z, Sun X P, Luo J, et al. Ultranarrow bandwidth tunable atomic filter via quantum interference-induced polarization rotation in Rb vapor[J]. Chinese Optics Letters, 2014, 12(12): 121404.
[20] Luo B, Yin L F, Xiong J Y, et al. Induced-dichroism-excited atomic line filter at 1529 nm[J]. IEEE Photonics Technology Letters, 2018, 30(17): 1551-1554.
[21] 何竹松, 掌蕴东, 刘双强, 等. 铷 775.9 nm 激光感生色散光学滤波器[J]. 中国激光, 2008, 35(4): 488-490.
He Z S, Zhang Y D, Liu S Q, et al. A rubidium laser induced dispersion optical filter at 775.9 nm[J]. Chinese Journal of Lasers, 2008, 35(4): 488-490.
[22] Gayen S K, Billmers R I, Yang G N, et al. Induced-dichroism-excited atomic line filter at 532 nm[J]. Optics Letters, 1995, 20(12): 1427-1429.
[23] He Z S, Zhang Y D, Wu H, et al. Theoretical model for an atomic optical filter based on optical anisotropy[J]. Journal of the Optical Society of America B, 2009, 26(9): 1755-1759.
[24] 张锦芳, 任雅娜, 王军民, 等. 铯原子激发态双色偏振光谱[J]. 物理学报, 2019, 68(11): 113201.
Zhang J F, Ren Y N, Wang J M, et al. Investigation of the two-color polarization spectroscopy between the excited states based on cesium atoms[J]. Acta Physica Sinica, 2019, 68(11): 113201.
[25] Carr C, Adams C S, Weatherill K J. Polarization spectroscopy of an excited state transition[J]. Optics Letters, 2012, 37(1): 118-120.
[26] Wang Y F, Zhang X G, Wang D Y, et al. Cs Faraday optical filter with a single transmission peak resonant with the atomic transition at 455 nm[J]. Optics Express, 2012, 20(23): 25817-25825.
[27] Yang B D, Gou Z Y, Wang J M, et al. Doppler-free dual-excited state spectroscopy and its application for measurement of hyperfine structure of $6D_{5/2}$ level of ^{133}Cs[J]. Applied Physics B, 2022, 128(11): 212.
[28] Fort C, Cataliotti F S, Raspollini P, et al. Optical double-resonance spectroscopy of trapped Cs atoms: hyperfine structure of the 8s and 6d excited states[J]. Zeitschrift Für Physik D Atoms, Molecules and Clusters, 1995, 34(2): 91-95.
[29] Yang B D, Zhang J F, Wang J M. Narrow linewidth two-color polarization spectroscopy due to the atomic coherence effect in a ladder-type atomic system[J]. Chinese Optics Letters, 2019, 17(9): 093001.
[30] Tanasittikosol M, Carr C, Adams C S, et al. Subnatural linewidths in two-photon excited-state spectroscopy[J]. Physical Review A, 2012, 85(3): 033830.
[31] Mohapatra A K, Jackson T R, Adams C S. Coherent optical detection of highly excited Rydberg states using electromagnetically induced transparency[J]. Physical Review Letters, 2007, 98(11): 113003.
[32] Chakrabarti A, Ray A. Exploring hyperfine levels of non-Rydberg excited states in a system using Autler-Townes splitting[J]. Applied Optics, 2020, 59(3): 735-741.
[33] Tao Z M, Zhang X G, Chen M, et al. Cs 728 nm excited state Faraday anomalous dispersion optical filter with indirect pump[J]. Physics Letters A, 2016, 380(25/26): 2150-2153.
[34] Xue X B, Tao Z M, Sun Q Q, et al. Faraday anomalous dispersion optical filter with a single transmission peak using a buffer-gas-filled rubidium cell[J]. Optics Letters, 2012, 37(12): 2274-2276.

Experimental Study on Ultra-narrow Bandwidth Optical Filters with Excited States of Cesium Atoms

Zhao Hanshuai[1], Yang Baodong[1,2,3*], Xue Zhao[1], Zheng Lanlan[1]

[1]*College of Physics and Electronic Engineering, Shanxi University, Taiyuan* 030006, *Shanxi, China*;
[2]*State Key Laboratory of Quantum Optics and Quantum Optics Device, Institute of Opto-Electronics, Shanxi University, Taiyuan* 030006, *Shanxi, China*;
[3]*Collaborative Innovation Center of Extreme Optics, Shanxi University, Taiyuan* 030006, *Shanxi, China*

Abstract

Objective Atomic optical filters have a broad range of applications in several areas, including atomic clocks, free-space optical communications, and laser remote sensing systems. The Faraday anomalous dispersion optical filter (FADOF) is one of the most popular optical filters because of its narrow bandwidth, high transmission, fast response, and high noise rejection. As a result, it has been intensively studied both theoretically and experimentally. The FADOF is based on the rotation of the polarization direction of a linearly polarized light signal when it passes through an atomic medium in a magnetic field. Most previously published studies have focused on the FADOF of the atomic transition between the ground and excited states; consequently, the selectivity of the operating wavelength of the FADOF is often limited. Some scholars have further investigated the FADOF between two excited states (ES-FADOF), owing to their abundant transitions. However, the bandwidths of the FADOF and ES-FADOF are usually of the order of ~GHz. Currently, the investigation of atomic optical filters with ultranarrow bandwidths remains a focus.

Methods Based on a ^{133}Cs $6S_{1/2}$-$6P_{3/2}$-$6D_{5/2}$ (852 nm+917 nm) ladder-type atomic system, we present an experimental study on a nonlinear optical filter with an ultra-narrow bandwidth, as shown in Fig. 1. A circularly polarized laser with a wavelength of 852 nm

was used as the pump light to populate the atoms from the ground state $6S_{1/2}$ to the intermediate excited state $6P_{3/2}$ and to polarize the atomic medium. The polarization direction of the 917 nm linearly polarized laser as the signal light, with a frequency in the vicinity of the $6P_{3/2}$-$6D_{5/2}$ transition, was rotated when it passed through the polarized atomic medium. The experimental setup is shown in Fig. 2. The temperature-controlled ^{133}Cs vapor cell was placed between a pair of Glan-Taylor prisms with perpendicular polarization directions; the extinction ratio of the prisms reached 100000∶1. The 852 nm pump and 917 nm signal lights overlapped in the ^{133}Cs vapor cell and were then separated by two dichroic mirrors. Subsequently, the signal light passed through an interference filter and reached a photodetector, enabling the realization of the induced dichroism excited atomic line filter (IDEALF) operating on the $6P_{3/2}$-$6D_{5/2}$ transition with an ultra-narrow bandwidth.

Results and Discussions The influences of parameters such as the temperature of ^{133}Cs vapor cell and the power of the 852 nm pump light on the peak transmittance and equivalent noise bandwidth (ENBW) of the IDEALF, are measured and analyzed. In particular, the difference in the IDEALF between the two experimental configurations is investigated when the 852 nm pump light is co-propagating or counter-propagating with the 917 nm signal light in the atomic medium. Notably, the Autler-Townes splitting phenomenon in the IDEALF spectral signal is observed for the counter-pumping configuration when the power of the 852 nm pump laser is relatively high (>4 mW), as indicated in Fig. 6, which is in good agreement with the theoretical calculation result using a simple model, as shown in Fig. 7. As a typical result, the IDEALF in the counter-pumping configuration has a higher peak transmission and narrow ENBW in comparison to that of the IDEALF in the co-pumping configuration (Fig. 5, Fig. 8, and Fig. 9). This is because the counter-pumping configuration is Doppler-free with an atomic coherence effect in a ladder-type atomic system, which has been confirmed in many other experiments, whereas the co-pumping configuration is an incoherent experimental system. The difference between the two experimental configurations causes a significant difference in the ENBW of the IDEALF. In our experimental parameters, the ENBW is in the range of ~7–60 MHz for the counter-pumping configuration and the ENBW in the range of ~90–140 MHz for the co-pumping configuration, and thus, the ENBW of the former is approximately half of the latter, as shown in Fig. 9.

Conclusions We demonstrate an IDEALF with ultra-narrow bandwidth in a ladder-type atomic system and compare its properties under two different experimental configurations. Under the optimized experimental parameters, the peak transmission of the IDEALF reaches ~20%. The ENBW of the IDEALF is at least one order of magnitude narrower than that of the FADOF (~GHz). The narrowest bandwidth of ~7 MHz of the IDEALF is realized, which is close to the natural linewidth of 5.2 MHz of the intermediate excited state $6P_{3/2}$. Under certain experimental conditions, the IDEALF signal exhibits two distinct profiles: a line-center filter with a single transmission peak is obtained for a co-propagating experimental configuration, and a line-wing filter similar to the popular FADOF is also realized in the case of a counter-propagating experimental configuration. Both of these profiles have significant application value in detecting weak light signals and eliminating the influence of background noise light, particularly in the case of a non-magnetic environment.

Key words optical filters; nonlinear optical effect; excited state; remote sensing